Journal of Engineering Science and Technology
Vol. 13, No. 4 (2018) 1070 - 1089

NUMERICAL INVESTIGATION OF FLOW FIELD IN PROTON EXCHANGE MEMBRANE FUEL CELL AT DIFFERENT CHANNEL GEOMETRIES

R. HADJADJ*, W. KAABAR

Department of Chemistry, Faculty of Pure Sciences,
University of Frères Mentouri Constantine 1, Algeria
*Corresponding Author: Razika.hadjadj@yahoo.fr

Abstract

This paper reports the three-dimensional modelling of a proton exchange membrane fuel cell (PEMFC) with straight flow field designs. Different shapes of both anode and cathode channels have been considered. Three geometrical configurations with same area: rectangular, triangular and elliptical straight channels are constructed to investigate the performance and the transport phenomena in the PEMFC at high and low operating voltages. The proposed model is a full cell, which includes different physical zones associated with a PEM fuel cell such as the Bipolar Plates (BPs) or current collectors, the flow channels, the Gas Diffusion Layers (GDLs), and the Catalyst Layers (CLs) on both anode and cathode sides as well as the membrane layer. The model is implemented into the commercial computational fluid dynamics (CFD) software package Fluent®6.3, with its user-defined functions (UDFs). The continuity, momentum, chemical species and charge conservation equations are coupled with electrochemical kinetics in the anode and the cathode channels and the Membrane Electrode Assembly (MEA). The obtained results determine that at high voltage (0.8 V) the cell performance is insensitive to the channel shape. The simulation results show that at low voltage (0.4 V) when anode and cathode channels geometry is triangular the performance of the cell is better than the rectangular and elliptical channels. The best performance is obtained for a triangular channel width of 0.1 mm.

Keywords: PEMFC, CFD, Fluent, Channel shape, Species distribution, Velocity field, Channel width.

Nomenclatures

a	Water activity
Cp	Specific heat capacity at constant pressure, J $kg^{-1}K^{-1}$
F	Faraday constant , 96487 C mol^{-1}
M	Molecular weight, $kgmol^{-1}$
P	Pressure, Pa
R	Gas constant , 8.314 J mol^{-1} K^{-1}
T	Temperature, K
V_{oc}	Open circuit voltage, V
y_j	Mass fraction of species j

Greek Symbols

α	Transfer coefficient , dimensionless
γ	Exponent for concentration dependence
ε	Porosity of the porous media
η	Activation overpotential
κ	Permeability, m^2
λ	Water content
μ	Viscosity, $kgm^{-1}s^{-1}$
$\vec{v}$	Velocity vector, ms^{-1}
ρ_g	Scalar density
τ	Stress tensor
ϕ	Phase potential

Abbreviations

BPs	Bipolar Plates
CFD	Computational Fluid Dynamics
CLs	Catalyst Layers
GDLs	Gas Diffusion Layers
PEM	Proton exchange membrane
PEMFC	Proton Exchange Membrane Fuel Cell
UDFs	User-Defined Functions

1. Introduction

The energy demands of this century face the depletion of fossil resources involving the search for alternative solutions. Renewable energy sources are predicted to grow rapidly in the near future, but are still limited for static applications (such as electricity generation and water desalination, etc.) [1, 2], and not yet envisaged for transportation applications. Hydrogen is thought to be the solution as a clean and renewable future energy vector [3, 4], meaning that it can be used as portable fuel. Hydrogen is the most common element in the universe, its use in fuel cells is effective by direct conversion of chemical energy into electrical energy.

To date, this is the cleanest energy converter, high performance, flexible and scalable in terms of power output. One type of fuel cell, a Proton Exchange Membrane fuel cell (PEMFC) supports the reaction between hydrogen and oxygen to produce electricity. It is considered one of the most promising technologies for both stationary and mobile applications. PEMFCs have high power density, solid

electrolyte, and low operating temperature, zero emission and quick start-up, as well as low corrosion [5]. They have greater efficiency when compared to heat engines and their use in modular electricity generation and propulsion of electric vehicles is promising [6, 7].A PEMFC is illustrated in Fig. 1.

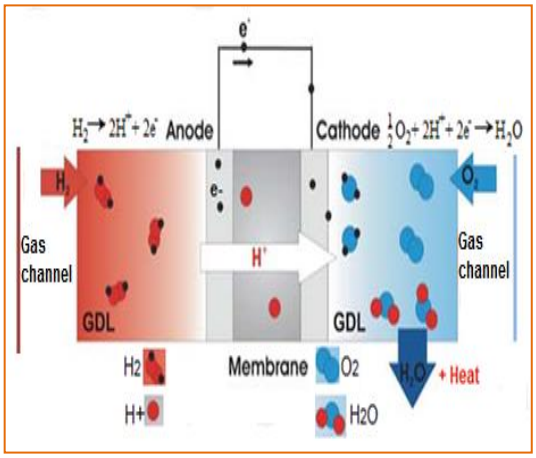

Fig. 1. Schematic representation of PEMFC system.

Fuel cell models represent a significant tool in the development of PEMFC technology, which facilitate understanding and optimizing their complex phenomena such as: fluid transfer mechanism (mass and heat), water management and electro-chemical reaction, etc., In the last years, computational fluid dynamic (CFD)software Package has proved to be a helpful tool, and has been frequently used to simulate the fuel cells behavior in various applications involving flow field, thermal and water management [8-13].

It is known that the flow field design in the bipolar plates plays a very important role for improving reactant utilization and liquid water removal in PEMFCs which enhance the fuel cell performance. The reactants, as well as the products, are transported to and from the cell through flow channels. In order to understand the effect of flow field design in transport performance in the PEM fuel cells, many research have been carried in various flow field configurations, including parallel, serpentine, interdigitated and other combined versions [14-22] and for different flow channel shapes such as semi-circular, trapezoidal, rectangular and triangular.

Ahmed et al. [23] investigated three different channel cross sections: rectangular, trapezoidal and parallelogram, on a straight flow channel at high current densities. Their results of the numerical simulations with these geometries revealed that the rectangular section channel provided the highest cell potentials, whereas the trapezoidal cross section displayed the most uniform current density distributions.

Kumar and Reddy [24] analyzed the effect of channel dimensions on the hydrogen consumption at the anode. For high hydrogen consumptions (80%), the optimum dimension values for channel width, rib width and channel depth were close to 1.5, 0.5 and 1.5 mm, respectively. Moreover, the effect of different channel shapes was investigated. They showed that triangular and hemispherical

shaped cross-section resulted in the highest hydrogen consumption by around 9% at anode, improving fuel cell efficiency.

Wang et al. [25] investigated numerically the effect of cathode channel shapes on the local transport characteristics and cell performance. The cells with triangle, trapezoid, and semicircle channels were examined and compared with rectangular channel. They suggested that the local transport phenomena in the cell indicates that triangle, trapezoid, and semicircle channel designs increase remarkably the flow velocity of reactant, enhancing liquid water removal and oxygen utilization.

Khazaee [26] studied experimentally and numerically single serpentine PEMFC performance with flow fields by changing the geometry of the channels. His results showed that when the geometry of the channel is rectangular the performance of the cell is better than the triangular and elliptical channels.

Ahmadi et al. [27] investigated the effect of increasing the width of the gas channel at the upper region, on the PEM fuel cell performance for straight flow channel. The cross section of the performance was obtained for inverse trapezoid channel with the 1.2 mm width in the top section of channel.

Zeng et al. [28] developed a three-dimensional, non-isothermal model with a single straight channel and used the genetic algorithm to study the optimization of channel configuration. They showed that, at an operating potential of 0.4 V, the optimal design obtained is a trapezoidal channel compared to a square channel.

To the best of our knowledge, no work has addressed the effect of both anode and cathode rectangular, triangular and elliptical channel shapes for a straight flow field on cell performance for two operating potential.

The operating conditions and electrochemical parameters used in this work are different from studies quoted in this paper.

In the present work, a complete three-dimensional, single phase and isothermal PEM fuel coupled with electrochemical reaction for a single straight PEMFC with three different channel shapes has been developed to investigate the internal physico-chemical processes and fluid flow distribution within a single cell unit. The electrochemical reactions, fluid mass transfer phenomena have been included in the cell model. The conservation equations are solved by using commercial computational fluid dynamics (CFD) software, Fluent® 6.3, and its PEMFC module.

The variation of gaseous species concentrations, distribution of current density and flow field over the cell unit are presented and discussed. Furthermore, the effects of changing the shapes of the flow channels are investigated by comparison between the three configurations at high and low voltage.

2. Numerical model

2.1. Model assumptions

Basic assumptions are made to simplify actual cell conditions in the theoretical model and thus facilitate the modelling approach of transport component influence on cell performance and transport phenomena. The following are the most important:

- The reactant and product are considered incompressible, ideal gas.
- The flow in channels and porous layers is laminar due to small pressure gradient and low flow velocities.
- The cell operates under steady-state condition (stationary condition).
- Isothermal condition (the cell temperature is uniform and fixed at 70°C = 343 K; it is the favourable temperature because it is in the range of 60°C-80°C).
- Butler -Volmer kinetics is used for electrochemical reaction rate [29].
- Water exists in vapor form only.
- The membrane is impermeable enough for gas phase to neglect diffusion of gases.
- Ohmic losses in the GDL and current collector are neglected.

2.2. Model equations

The transport of gas mixtures in different parts of PEM fuel cell is governed with standard equations of fluid mechanics (conservation of mass or continuity conservation, momentum, species transport) [29]. These equations were coupled to the electrochemical model which consisted in two potential equations associated to the electron transport and another potential equation describing the proton transport (charge equations).

- **Continuity equation**

$$\frac{\partial(\rho_g)}{\partial t} + \nabla\left(\rho_g \vec{v}\right) = S_m \tag{1}$$

S_m is the mass source term. For all zones in this model, S_m= 0.

- **Momentum conservation equation**

$$\frac{\partial \rho_g \vec{v}}{\partial t} + \nabla\left(\rho_g \vec{v}\vec{v}\right) = -\nabla p + \nabla\tau + S_M \tag{2}$$

The momentum equation shown in Eq. (2) is used to solve the velocities of the fluid in the channels and the GDL and the species partial pressures.

S_M is the momentum source term. S_M = 0 for the gas channels, for the porous medium (gas diffusion layers and the catalyst layers). Equation (3) defines the source term S_M as follows:

$$S_M = -\frac{\mu}{\kappa}\varepsilon\vec{v} \tag{3}$$

- **Species conservation equation**

The species transport equation is defined as follows according to Fick's law:

$$\frac{\partial(\varepsilon\rho_g y_j)}{\partial t} + \nabla\left(\rho_g \vec{v} y_j\right) = \nabla\left(\rho_g D_j^{eff} y_j\right) + S_j \tag{4}$$

where D_j^{eff} is the effective mass diffusivity. In Fluent, D_j^{eff} is calculated according to Eq. (5) accounting for the effects of temperature, pressure and water saturation.

$$D_j^{eff} = \varepsilon^{1.5}(1-s)^{r_s} D_j^0 \left(\frac{P_0}{P}\right)^{\gamma_p} \left(\frac{T}{T_0}\right)^{\gamma_t} \tag{5}$$

where D_j^0 is the mass diffusivity of species j at reference temperature and pressure (P_0, T_0) [30].

S_j is the species volumetric source terms, $S_j = 0$ for the channels, the gas diffusion layers and the membrane. For the catalyst layers, the source terms of hydrogen, oxygen and water the species volumetric source terms are as follows:

Hydrogen consumption at anode

$$S_{H_2} = -\frac{M_{H_2}}{2F} J_a$$

Oxygen consumption at cathode

$$S_{O_2} = -\frac{M_{O_2}}{4F} J_c$$

Water vapor production at cathode

$$S_{H_2O} = \frac{M_{H_2O}}{2F} J_c$$

Water vapor net transport from anode to cathode

$$S_{H_2O} = -\delta \frac{M_{H_2O}}{F} J_a$$

J is the transfer current density (A/m^3) can be calculated from Butler-Volmer function as shown in Eqs. (6) and (7) [31].

$$J_a = J_a^{ref} \left(\frac{C_{H_2}}{C_{H_2}^{ref}}\right)^{\gamma_a} \left[\exp\left(\frac{\alpha_a F}{RT}\eta_a\right) - \exp\left(\frac{\alpha_c F}{RT}\eta_a\right)\right] \tag{6}$$

$$J_c = J_c^{ref} \left(\frac{C_{O_2}}{C_{O_2}^{ref}}\right)^{\gamma_a} \left[-\exp\left(\frac{\alpha_a F}{RT}\eta_c\right) + \exp\left(\frac{\alpha_c F}{RT}\eta_c\right)\right] \tag{7}$$

- **Energy conservation equation**

We have the following equation for energy conservation

$$\frac{\partial(\varepsilon\rho_g C_P T)}{\partial t} = \nabla\left(\varepsilon\rho_g C_P \vec{v} T\right) = \nabla\left(K^{eff} \nabla T\right) + S_e \tag{8}$$

S_e is the volumetric source term and is defined for all zones of the cell by Eq. (9).

$$S_e = h_{react} - \eta R_{a,c} + I^2 R_{ohm} + h_L \tag{9}$$

In this equation, I^2R_{ohm} is the ohmic heating term, h_{react} is the heat of formation of water term, $\eta R_{a,c}$ is the electric work term, and h_L is the latent heat of water term.

2.2.5. Charge conservation equations

- **Electron transport equation**

$$\nabla(\sigma_{sol}\nabla\Phi_{sol})+J_{sol}=0 \tag{10}$$

- **Proton transport equation**

$$\nabla(\sigma_{mem}\nabla\Phi_{mem})+J_{mem}=0 \tag{11}$$

where J_{sol} and J_{mem} are the source terms of solid phase and membrane phase. These terms are only defined in the catalyst layers:

For the solid phase: $J_{sol}=-J_a(<0)$ Anode side

$J_{sol}=J_c(>0)$Cathode side

For the membrane phase: $J_{mem}=J_a(>0)$ Anode side

$J_{mem}=-J_c(<0)$ Cathode side

2.2.6. Water transport through membrane

Since PEM fuel cell operates under relatively low temperature (< 100°C), the water vapor may condense to liquid water, especially in high current densities. In the present model the water in the assumption of single phase model is used. It means the water in the membrane is assumed to be in vapor state and there is no liquid in the fuel cell (liquid water is ignored).

Water content in membrane, λ [32].

$$\lambda=\begin{cases}0.043+17.81a-39.85a^2+36a^3 & 0\le a\le 1\\ 14+1.4(a-1) & 1<a\le 3\end{cases} \tag{12}$$

a is the water activity in gas phase: $a=\dfrac{c_w}{P^{sat}}RT$

where c_w and P^{sat} are concentration and saturation pressure of water vapor at each electrode respectively, the saturation pressure, P^{sat}, is computed as [33]:

$$\log_{10}P^{sat}=-2.1794+0.02953(T-273.15)-9.1837\times10^{-5}(T-273.15)^2 +1.4454\times10^{-7}(T-273.15)^3 \tag{13}$$

2.3. Model description and mesh generation

The objective model geometry studied in the present work is shown in Fig. 2. The same straight and parallel channels flow field of the polar plate was assumed on the cathode and anode side. The multi-channel structure and the periodicity of the polar plate make it possible to select one unit cell with dimensions of $x\times y\times z$ = $2\times4.48\times125$ mm^3.

The computational domain includes all major cell components for full cell modeling (BP, flow channel, GDLs, CLs and membrane). A commercial Nafion117 was employed as a proton exchange membrane (PEM) [34].The detailed dimensions are shown in Table 1. The complete 3D grid model (computational grids) of PEM fuel cell with three different cross sectional shapes

(rectangular, triangular and elliptical) was prepared and meshed with a pre-processing software Gambit®2.4.6 [29], as shown in Fig. 2(d).The utilized grid was verified to give mesh independent results.

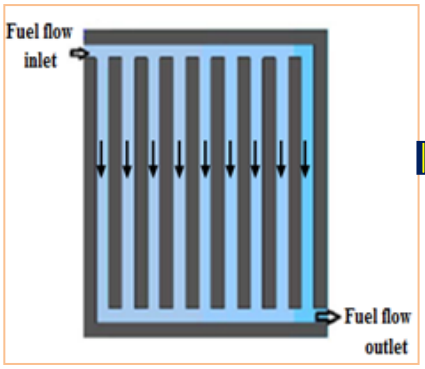

(a) Top view of a single straight channel flow field.

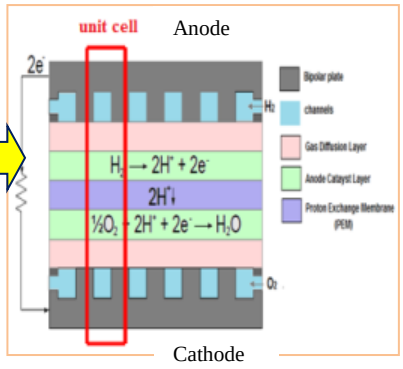

(b) Cross-sectional view.

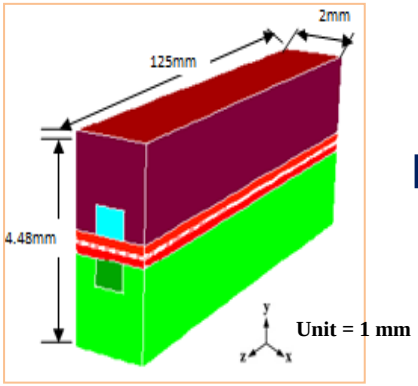

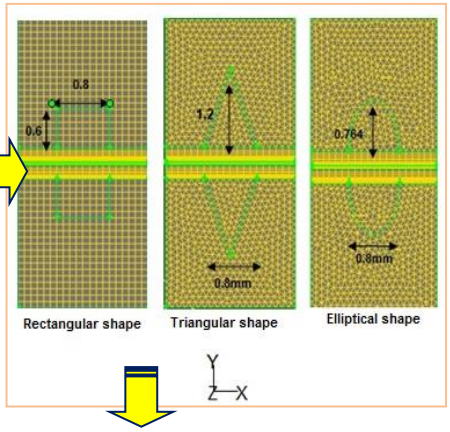

(c) Unit cell dimensions.

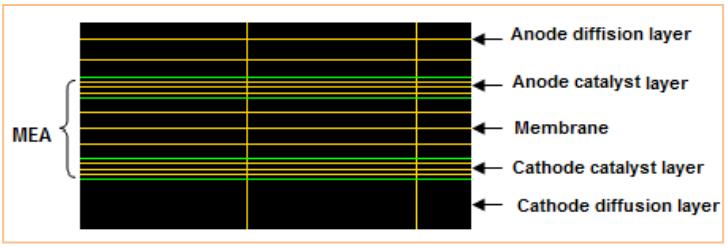

(d) Mesh generation of three geometries.

Fig. 2. Single straight channel in PEM fuel cell with mesh generation of three geometries.

Table 1. Model geometry and operating conditions.

Parameter	Value
Model /Cell width, m	2×10^{-3}
Model / Cell height, m	4.48×10^{-3}
Model /Cell length, m	125×10^{-3}
Gas Channel width, m	8×10^{-4}
Gas Channel height, m	6×10^{-4}
Membrane (Nafion 117) thickness, m	36×10^{-6}
Catalysts layers thickness, m	12×10^{-6}
Gas diffusion layers thickness, m	21×10^{-5}
Current collectors width, m	2×10^{-3}
Current collectors height, m	2×10^{-3}
Cell Temperature (T_{cell}), K	343
Operating pressure (P_{cell}), atm	2
Open-circuit-voltage (V_{oc}), V	1.1

2.3.1. Boundary conditions

The boundary conditions used for the CFD model are based on publication [36]. The channel inlet is defined as a mass-flow-inlet of the gas mixture. The mass flow rates (H_2/O_2 (air)) are calculated for a stoichiometry of ζ_a = 2, ζ_c= 2 at a reference current density of 1 A/cm^2; the channel outlet is defined as a pressure outlet. The channel faces which are adjacent to the gas diffusion layers and the faces of the gas diffusion layers that are next to the catalyst layers are defined as a porous jump (porous media). The direction for H_2 and O_2 is defined as counter-current flow pattern. The cell is fed with mixture H_2/H_2O and O_2 /H_2O at the anode and the cathode inlet respectively. It is operated at P_{cell} = 2 atm and T_{cell} = 343 K, under an isothermal assumption. The cases are simulated under the low humidity inlet operation (relative humidity RH= 47%).

2.3.2. Operating conditions

The operating conditions and parameters related to electrochemical kinetics are presented in Tables 1 and 2.

The reference cell open-circuit voltage V_{oc}=0.0025 T_{cell}+ 0.2329 [37].

2.4. Numerical solution method and strategy

The CFD code Fluent is used to achieve the simulation. This software package provides a solver for fluid-flow, heat-transfer, chemical-reaction and related problems ranging in complexity from two-dimensional single phase and steady state, to three-dimensional multi-phase and transient. The computational domain is divided into control volumes and Fluent is used to solve the three-dimensional conservation equations, using appropriately specified boundary conditions in finite-volume form.

The numerical simulation model used to solve the governing equations is based on the semi-implicit method for pressure linked equations (SIMPLE) algorithm developed by Patankar [38].The source terms generated by the

electrochemical reaction are inserted into the mass, momentum and species conservation equations in different zones of the fuel cell using a User Define Function (UDF included in Fluent code; Fuel Cell Module).

The solution is obtained by solving the coupled set of conservation equations, Eqs. (1) to (13), explicitly using a finite volume approach, this method is based on the iteration processes and the solution was considered to be convergent when the relative error in each field between two consecutive iterations was less than 10^{-3} for all variables and 10^{-6} for energy equation.

The calculations finally generate different parameters: species, current density and flow field distributions, these parameters judge the best cross-section shape for the best fuel cell performance.

Table 2. Electrochemical parameters.

Parameter	Symbol	Value	Reference
Anode			
Gas	Hydrogen (H_2)		
Ref. exchange current density, A/m^3	j_a^{ref}	1×10^9	[35]
Ref. concentration, kmol/m^3		1.0	[35]
Concentration exponent	γ_a	0.5	[35]
Exchange coefficient	α_a	2.0	[35]
Reference diffusivity, m^2/s	$D^0_{H_2}$	11×10^{-5}	[30]
	$D^0_{H_2O}$	7.35×10^{-5}	[30]
	Other species	1.1×10^{-5}	[30]
Mass fraction of H_2	y_{H2}	0.727	[39]
Mass fraction of H_2O	y_{H2O}	0.273	[39]
Cathode			
Gas	Air		
Ref. exchange current density, A/m^3	j_c^{ref}	25.85×10^4	[40]
Ref. concentration, kmol/m^3		1.0	[35]
Concentration exponent	γ_c	1.0	[35]
Exchange coefficient	α_c	2.0	[35]
Reference diffusivity, m^2/s	$D^0_{O_2}$	3.2×10^{-5}	[30]
Mass fraction of oxygen	y_{O2}	0.225	[39]
Mass fraction of H_2O	y_{H20}	0.024	[34]
Mass fraction of nitrogen	y_{N2}	0.751	
Porosity of diffusion layer	ε_d	0.55	[30]
Porosity of catalyst layer	ε_l	0.457	[30]
Porosity of membrane	ε_m	0.28	[41]

3. Results and Discussion

The distribution of gas composition, current density and flow field for three channel configurations in counter-current flow cells operating at high and low voltages are presented and discussed below.

3.1. Model validation

The validation of the numerical results is performed by comparing the present model with results obtained in experimental data reported by [42]. Figure 3 shows the comparison of the numerical and experimental results of the cell performance, i.e., the operation voltage V_{cell} versus the current density of fuel cells I(Acm^{-2}), at the operating conditions of low humidified fuel gases with pressure of 1atm, and operating temperatures of 70 °C.

The comparison indicates that, at low current density, the results from modeling simulation are in favorable agreement with experimental data, at high current densities, the results of experimental data have higher value compared to the simulated results due to the some difference in physical parameters, i.e., reactants inlet boundary conditions, relative humidity of gases, coefficient stoichiometric of anode and cathode…etc.

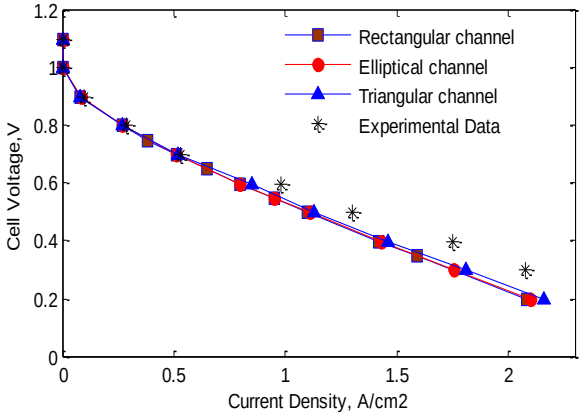

Fig. 3. Model validation with experimental data.

3.2. Polarization curve (I-V)

The performance of the fuel cell system characterized by the current-voltage curve (polarization curve) depends on several factors and operating parameters implemented into the model, such as the geometry of the flow paths in the bipolar plates. In order to plot the (I-V) curve, the base operating parameters considered are the following: The operating pressure and temperature of both anode and cathode are 1atm and 343 K, the mass flow rates are calculated for $\zeta_a = 2$, $\zeta_c = 2$, the RH = 47% in anode of hydrogen gas and the cathode of air.

Figure 4 shows the comparison of polarization curves of the PEMFC for the three models proposed. It can be seen that globally there is very little difference for the polarization curve behavior between the three shapes of channels. However, under further observation at current density of more than 1.5A/cm^2, it could be seen that triangular channel shows slightly higher cell potential compared to other channels. Polarization (I-V) curve, which is an insufficient approach for the comprehensive assessment of PEMFC models. Therefore, changing channel shape indeed affects the polarization curve, while no sharp conclusion could be drawn yet from this preliminary study.

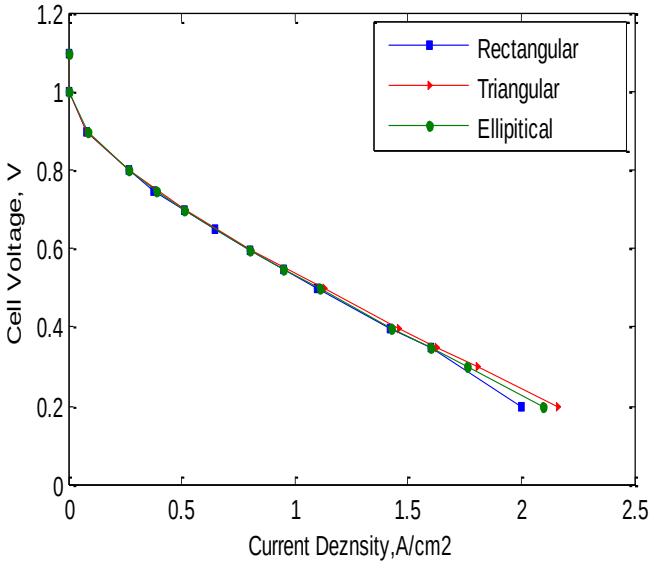

Fig. 4. Polarization curves for PEM fuel cell with various flow channel shapes.

3.3. Species distribution

Species distribution of H_2 at anode, O_2 at cathode and H_2O_{vapor} at cathode catalyst layer are investigated.Knowing that the direction of inlet gasses is assumed on counter-flow direction, the gas inlet is located at z = 125(upper) at anode and at z = 0 for Cathode (lower).

A global view in 3D distribution of the effect of channel shape design on hydrogen and oxygen mass fraction along the anode and cathode respectively, at 0.4 V and 0.8 V is shown in Figs. 5 and 6 for three flow channel shapes, while in Fig. 7 hydrogen and oxygen distributions at catalyst surface are presented for the cell voltage 0.4 V

Generally, the mass fraction of oxygen and hydrogen decreases gradually from the channel toward the catalyst surface where reaction consumption takes place. At low cell voltage (0.4 V), the mass fraction of both species decreases rapidly. In diffusion and catalyst surface the mass fraction of oxygen reaches the zero value, thus, more oxygen is required for the electrochemical reaction.

At 0.8 V, the hydrogen and oxygen concentration are relatively more uniform and the mass transfer is low that reduces the consumption rate of both reactants. The channel shape is seen to have little effect on the cell performance.

At catalyst layer surface (Fig. 7) the influence of channel shape becomes obvious at 0.4 V. The consumed hydrogen at anode (or oxygen at cathode), can be determined from the hydrogen (or oxygen) mass fraction difference from inlet to outlet. It can be seen from Fig.7 that the highest hydrogen and oxygen consumption rate occurs at the triangular channel compared to rectangular and elliptical channels. This result agrees with that of Kumar et al. [24] who showed that triangular shaped cross-section increased hydrogen consumption at anode.

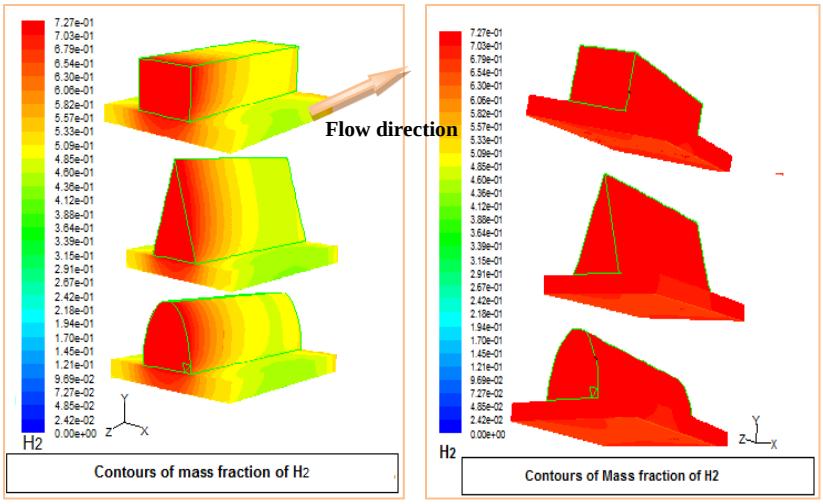

Fig. 5. Concentration distribution of hydrogen for various anode channel shapes at a) 0.4 V and b) 0.8 V.

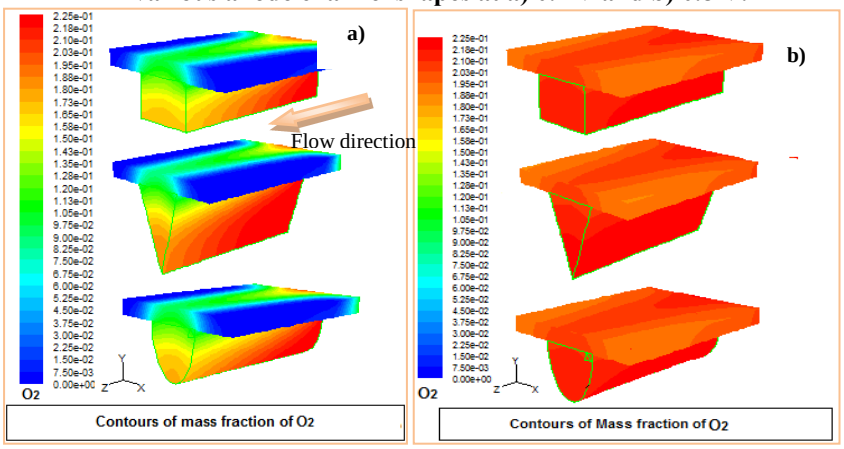

Fig. 6. Concentration distribution of oxygen for various cathode channel shapes at a) 0.4 V and b) 0.8 V in counter-current flow pattern.

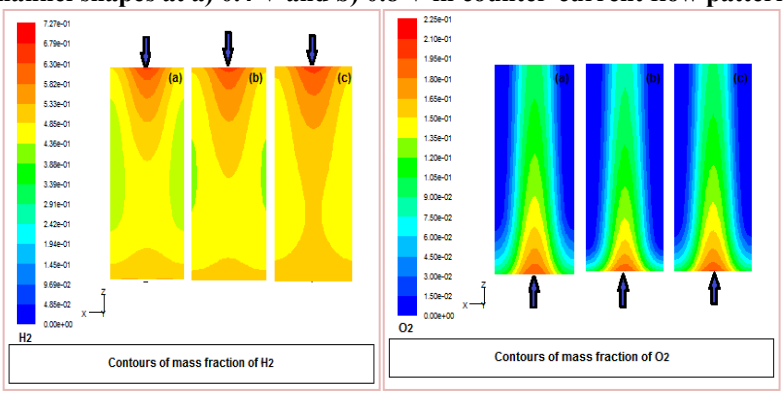

Fig. 7. Hydrogen and oxygen concentration at cathode catalyst layer at 0.4 V, for (a) rectangular (b) triangular, (c) elliptical channels.

Figure 8 shows 3D water vapor distribution and water vapor distribution at cathode catalyst layer for the three geometries at cell voltages 0.4 V for Fig. 8(A) and 0.8 V for Fig. 8(B).

It is clearly seen that the water concentration is very weak at the inlet; the cathode flow remains dry since only a little amount of water arrives from the anode (electro-osmotic flow).Then, the water vapor concentration increases gradually until it reaches its maximum at the outlet.

A large amount of water occurs at cell voltage of 0.4 V, as water is coming from the anode and is produced by Oxygen Reduction Reaction (ORR) in the cathodic half-cell reaction at the surface of catalyst layer. It can be shown that at 0.4 V the water rate formed in triangular channel is approximately 5% higher than in rectangular and elliptical channels (5×10^{-3} kmol/m^3 for triangular compared with 4.93×10^{-3} kmol /m^{3}and 4.95×10^{-3} kmol/m^3 for rectangular and elliptical respectively).

At low cell voltages (Fig. 8(A)) water production on the cathode side is sufficient to maintain good proton conductivity for all the simulated shape geometries.

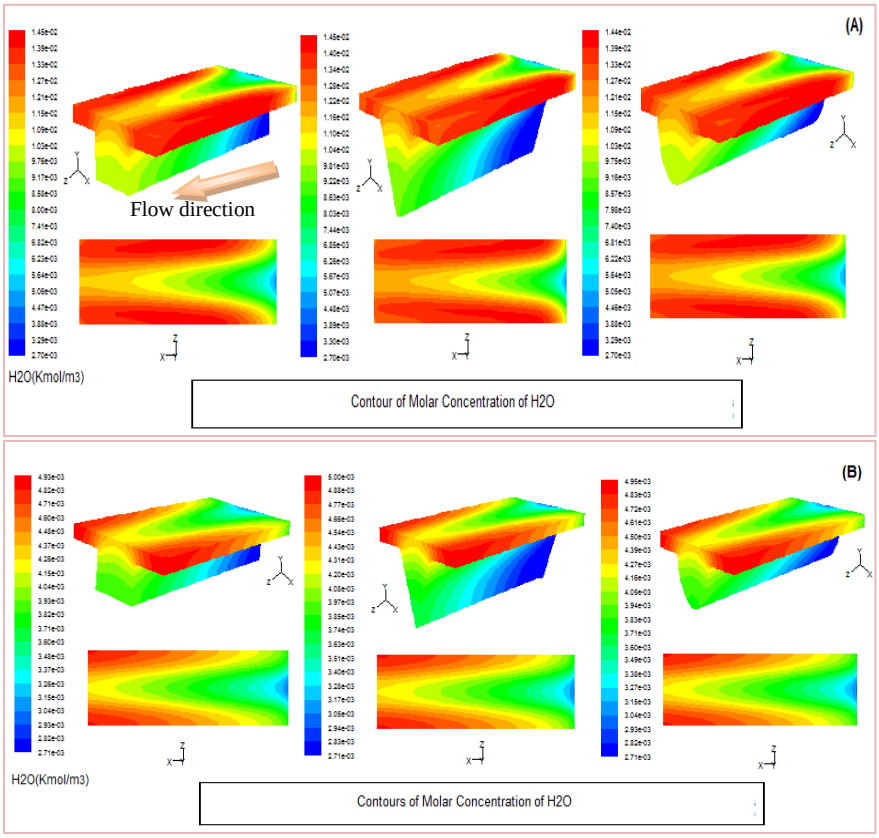

Fig. 8.Water vapour distribution: 3D and at cathode catalyst surface for the three geometries, at (A) V_{cell} = 0.4 V and (B) V_{cell} = 0.8 V.

3.4. Current density distribution

Because the channel shape starts to differ at low voltage the current densities distribution, velocities field and effect of channel width we analyzed at cell

voltage V_{cell} = 0.4 V.The predicted current density profiles in the catalyst layer along the cell length at 0.4 V are presented in Fig. 9.

At the beginning part (z = 0), the current density for all three channel shapes increases gradually with increases in direction Z. Then the increase becomes sharp due to strong oxygen consumption at the catalyst layer by the electrochemical reaction at the first of the channels. Maximum values of current densities are reached at different positions within the cell: 44510Am^{-2} at Z = 15 mm for the triangular channel; 42687 Am^{-2} at Z = 27 mm for rectangular channel and 43573Am^{-2} at Z = 24 mm for elliptical channel.

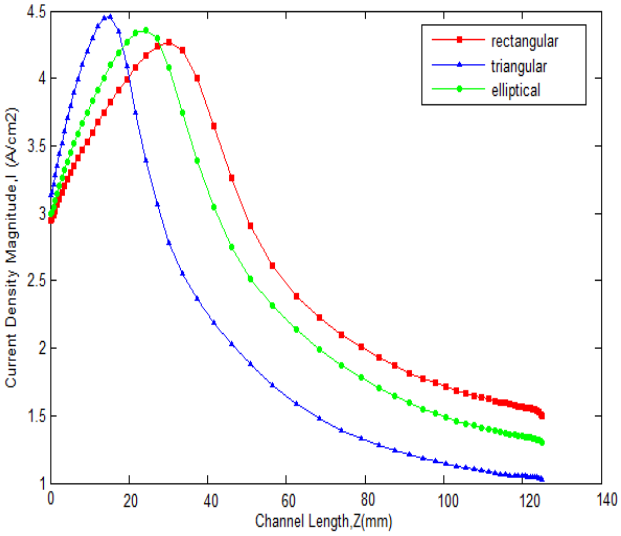

Fig. 9. Current density distribution at cathodic catalyst surface along the *Z* direction for the three models proposed at V_{cell} = 0.4 V.

This can be explained this by the difference in the rate of oxygen consumption at the catalyst surface as shown in Fig. 7. Then the current density decreases until Z = 125 mm due to the reduction in concentration of the oxygen by consuming it along the channel. According to Eqs. (6) and (7), current density is proportional to the consumed concentration of the reactants. Also it can be seen that the cumulative current densities value for rectangular channel is the best one compared with triangular and elliptical channel.

3.5. Flow field distribution

The transport phenomena in the flow channel, as well as in the gas diffusion layer of a fuel cell, are important. The velocity vectors of the gas mixture within the PEM fuel cell are shown in Fig. 10. Clearly, the velocity magnitude is uniform at the channel inlet due to the viscosity (a boundary layer has been developed in the wall of the channel and the interface of GDL), therefore the flow becoming fully developed within the channels where the maximum value is located at the central core of the flow channel and the lateral velocities are quickly reduced. This profile is maintained until the channel outlet. It is important to note that the velocity field is very weak in the porous medium (GDLs, CLs, PEM) because of

reduction in transport rate in these layers. For all three designs, it can be seen that the highest velocity magnitude is found in the triangular channel (22.6 m/s for triangular channel compared with 19.7 m/s and 20.9 m/s for rectangular and elliptical channels respectively).

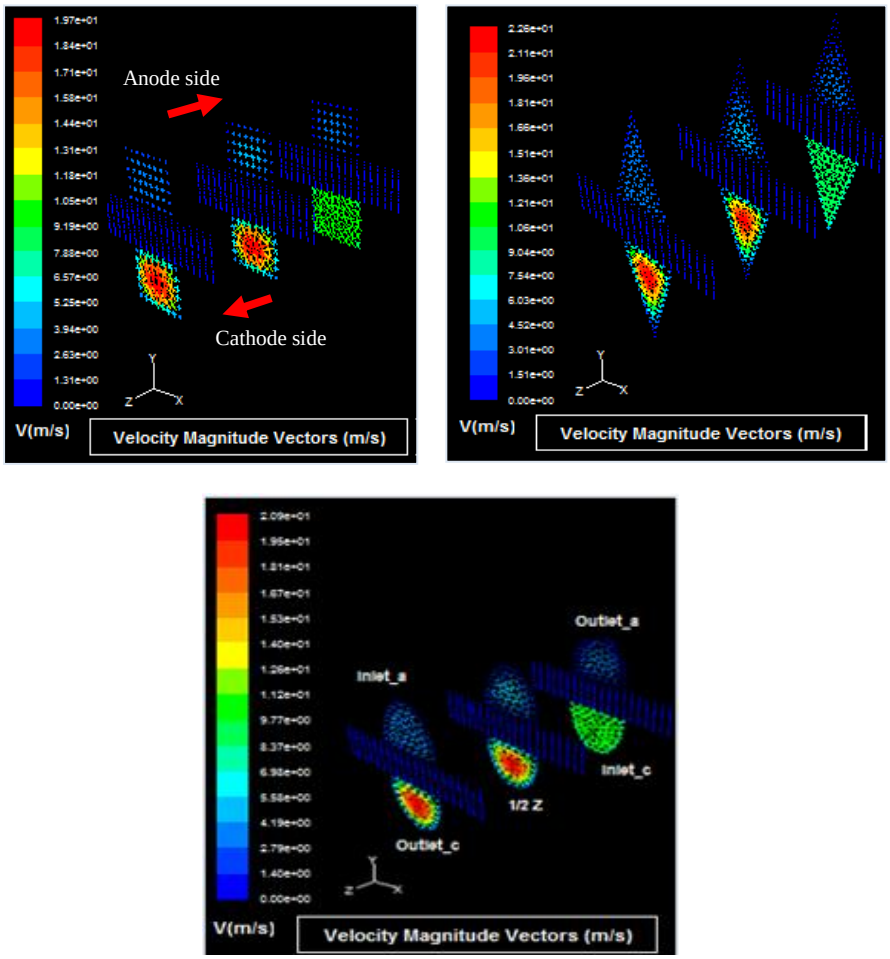

Fig. 10.Velocity field vectors of gas mixture inside the cell at V_{cell} = 0.4 V.

3.6. Effect of channel width

The channel size is a major factor which can affect the cell performance through the distribution of reactant and product gas species in channels, the diffusion within the GDL and the active surface where the chemical reaction takes place (contact surface area). Figure 11 shows profiles of hydrogen and oxygen concentrations at catalyst layer using triangular straight channels with different widths: 0.1 mm, 0.3 mm, 0.5 mm, 0.7 mm and fixed height = 0.6 mm.

Mass fraction profiles of hydrogen in anode catalyst layer along the length of the cell are shown in Fig. 11 (Left). Due to the oxidation reaction in anode catalyst layer, where the hydrogen diffuses and consumed along the flow

direction, the concentration of H_2 dropping from the maximum amount at the inlet (z = 0.125 m) to the lowest point at the outlet (z = 0). Therefore, the difference between the four profiles is clearly observed, the net consumption of hydrogen (mass fraction difference from inlet to outlet) is highest when the channel width is 0.1 mm (4.2×10^{-1} to 1.7×10^{-1}) compared with lowest consumption when the width is 0.7 mm (4.1×10^{-1} to 3.8×10^{-1}).

The concentration profiles of consumed oxygen are illustrated in Fig. 11 (Right). It is clear that the oxygen concentration decreases along the flow direction from inlet (z = 0) to outlet (z = 0.125 m), where oxygen has been consumed producing water during electrochemical reaction with hydrogen. The high net consumed oxygen is in the channel of width 0.1 mm (2.04×10^{-1} to 1.71×10^{-10}), and the bad consumption is within the channel of width 0.7 mm (1.9×10^{-1} to1.1×10^{-1}).

Accordingly, the results show that as the channel width increases, the mass fractions of H_2/O_2 are lowered as a consequence of the highly reduced average current density.

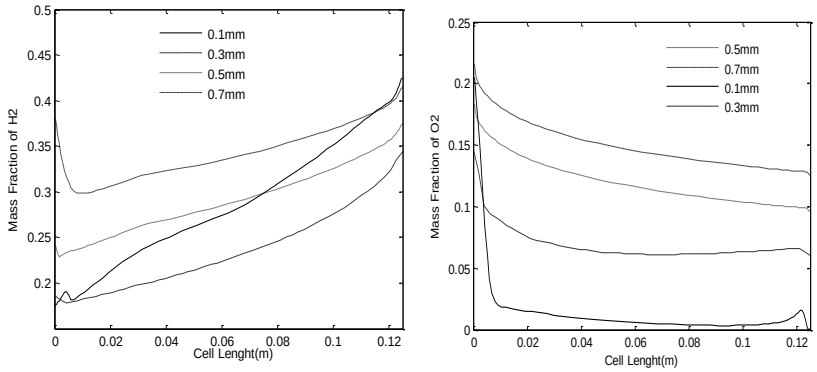

Fig. 11. Effect of triangular channel width on hydrogen and oxygen concentrations at catalyst layer; Hydrogen (left), Oxygen (right) at V_{cell} = 0.4 V.

4. Conclusion

A computational three-dimensional single phase model of a PEMFC with straight channel geometry for predicting the effect of different channels shapes was developed. Simulations were performed using the commercial computational fluid dynamics software Fluent and its PEMFC module. The main objective of this study was to investigate the cell performance at high and low operating voltage for three different channel configurations with same area (rectangular, triangular and elliptical) at cathode and anode. The effect of channel width on hydrogen and oxygen consumption was investigated for 0.1 mm, 0.3 mm, 0.5 mm and 0.7 mm.

Simulations results revealed that at cell voltage of 0.8 V the cell performance was insensitive to the channel shape. Whereas, at 0.4 V the effect of changing channel geometries became apparent. The results showed that the effect of channel shapes was similar between the anode and cathode sides. The high hydrogen and oxygen consumption rates occurred at the triangular channel, and the water rate formed in this channel was approximately 5% higher than in rectangular and elliptical ones.Moreover, the results indicated that local density

and velocity distributions at cathode were strongly dependent on channel shapes. The highest velocity magnitude of the gas mixture was encountered in the triangular channel. Based on triangular shaped channel, the simulations showed that high reactant consumption was obtained for 0.1 mm channel width.

Clearly, in this model, a high performance was observed by using a triangular geometry for the channels of both anode and cathode with an optimum width of 0.1 mm.

References

1. Behl, R.K.; Chhibar, R.N.; Jain, S.; Bahl, V.P.; and ElBassam, N. (2012).*Renewable energy sources and their applications*. AGROBIOS international.
2. Goosen, M.; Mahmoudi, H.; Ghaffour, N.; and Sablani, S.S. (2011).*Application of Renewable Energies for Water Desalination*. Croatia: InTech Europe.
3. M'batna, J.P.(2011). *Contribution à la modélisation tridimensionnelle du comportement thermo fluidique d'une cellule de pile à combustible à membrane échangeuse de protons*. Ph.D. Thesis. Sciences Pour l'Ingénieur et Microtechniques. Université de Technologie de Belfort-Montbéliard et de l'Université de Franche-Comté, France.
4. Boudellal, M. (2007). *La pile a combustible (Structure, fonctionnement, application*). Paris: Dunod.
5. Pukrushpan, T.; Stefanopoulou, G.; and Peng, H. (2004). *Control of fuel cell power systems*. London: Springer.
6. Kordesch, K.; and Simander, G. (1996). *Fuel Cells and Their Application*. Federal Republic of Germany: Weinheim.
7. Wang, H.; Yuan, X.; and Li, H. (2012). *PEM Fuel Cell Diagnostic Tools*. New York: Tayor & Francis Group.
8. Phong, T.N.; Torsten, B.; and Djilali, N. (2004**)**. Computational model of a PEM fuel cell with serpentine gas flow channels. *Journal of Power Sources*, 130, 149-157.
9. Kuo, J.K.; and Chen, C.K. (2007).The effects of buoyancy on the performance of a PEM fuel cell with a wave-Like gas flow channel design by numerical investigation. *International Journal of Heat and Mass Transfer*, 50, 4166-4179.
10. Dutta, S.; Shimpalee, S.; and Van Zee, J.W. (2000). Three-dimensional numerical simulation of straight channel PEM fuel cells. *Journal of Applied Electrochemistry*, 30,135-145.
11. Carcadea, E.; Ingham, D.B.; Stefanescu, I.; Ionete, R.; and Ene, H. (2011). The influence of permeability changes for a 7-Serpentine channel PEM fuel cell performance. *International Journal of Hydrogen Energy*, 36, 10376-10383.
12. Jeon, D. H.; Kim, K.N.; Baek, S. M.; and Nam, J.H. (2011). The effect of relative humidity of the cathode on the performance and the uniformity of PEM fuel cells. *International Journal of Hydrogen Energy, 36*, 12499-12511.

13. Berning, T.; and Djilali, N. (2003). Three-dimensional computational analysis of transport phenomena in a PEM fuel cell-a parametric study. *Journal of Power Sources*, 124(2), 440-452.
14. Salva, J.A.; Tapia, E.; Iranzo, A.; Pinoa, F.J.; Cabrera, J.; Rosa, F. (2012). Safety study of a hydrogen leak in a fuel cell vehicle using computational fluid dynamics. *International Journal of Hydrogen Energy*, 37, 5299-5306.
15. Liu, X.; Tao, W.; Li, Z.; and He, Y. (2006). Three-dimensional transport model of PEM fuel cell with straight flow channels. *Journal of Power Sources*, 158, 25-35.
16. Manso, A.P.; Marzo, F.F.; Barranco, J.; Garikano, X.; and Garmendia Mujika, M. (2012). Influence of geometric parameters of the flow fields on performance of a PEM fuel cell. *International Journal of Hydrogen Energy*, 37, 15256-15287.
17. Han, Y.; and Zhan, J.M. (2010). The impact of channel assembled angle on proton exchange membrane fuel cell performance. *Journal of Power Sources*, 195, 6586-6597.
18. Jeon, D.H.; Greenway, S.; Shimpalee, S.; and Van Zee, J.W. (2008). The effect of serpentine flow-field designs on PEM fuel cell performance. *International Journal of Hydrogen Energy*, 33, 1052-1066.
19. Li, X.; and Sabir, I. (2005). Review of bipolar plates in PEM fuel cell: Flow-field designs. *International Journal of Hydrogen Energy*, 30, 359-371.
20. Wang, X.D.; Yan, W.M.; Duan, Y.Y; Weng, F.B; Jung, G.B; and Lee, C.Y. (2010). Numerical study on channel size effect for proton exchange membrane fuel cell with serpentine flow field. *Energy Conversion and Management*, 51, 959-968.
21. Wang, X. D.; Duan, Y.Y; Yan, W.M.; and Peng, X.F. (2008). Effect of flow channel geometry on cell performance for PEM fuel cell with parallel and interdigitated flow fields. *Electrochimica Acta*, 53, 5334-5343.
22. Jeon, D.H.; Greenway, S.; Shimpalee, S.; and Van Zee, J.W. (2008). The effect of serpentine flow-field designs on PEM fuel cell performance. *International Journal of Hydrogen Energy*, 33, 1052-1066.
23. Ahmed, D.H.; and Sung, H.J. (2006). Effects of channel geometrical configuration and shoulder width on PEMFC performance at high current density. *Journal of Power Sources*, 162(1), 327-339.
24. Kumar, A.; and Reddy, R.G. (2003).Effect of channel dimensions and shape in the Flow-Field distributor on the performance of polymer electrolyte membrane fuel cells. *Journal of Power Sources*, 113(1), 11-18.
25. Wang, X. D.; Lu, G.; Duan, Y.Y.; and Lee, D.J. (2012). Numerical analysis on performances of polymer electrolyte membrane fuel cells with various cathode flow channel geometries. *International Journal of Hydrogen Energy*, 37(20), 15778-15786.
26. Khazaee, I. (2015). Experimental investigation and numerical comparison of the performance of a proton exchange membrane fuel cell at different channel geometry. *Heat and Mass Transfer*, 51(8), 1177-1187.
27. Ahmadi, N.; Rezazadeh, S.; Dadvand, A.; and Mirzaee, I. (2017). Study of the effect of gas channels geometry on the performance of polymer

electrolyte membrane fuel cell. *Periodica Polytechnica Chemical Engineering*, 62(1), 97-105.

28. Zeng, X.; Ge, Y.; Shen, J.; Zeng, L.; and Liu, Z. (2017). The optimization of channels for proton exchange membrane fuel cell applying genetic alogorithm. *International Journal of Heat and Mass Transfer*, 105, 81-89.
29. Fluent 6.3. (2006). *Fuel cell Modules Manual*, from http://www.fluent.com.
30. Wei, Y.; Yong, T.; Pan, M.; Li, Z. L.; and Tang, B. (2010). Model prediction of effects of operating parameters on proton exchange membrane fuel cell performance. *Renewable Energy*, 35, 656-666.
31. Dokkar, B.; Settou, N.E.; Imine, O.; Saifi, N.; Negrou, B.; and Nemouchi, Z.(2011). Simulation of species transport and water management in PEM fuel cell. *International Journal of Hydrogen Energy*, 36, 4220-4227.
32. Berning, T., Lu, D.M.; and Djilali, N. (2002). Three-dimensional computational analysis of phenomena in a PEM fuel cell. *Journal of Power Sources*, 106, 284-294.
33. Kazi, S.N. (2012). *Heat transfer phenomena and application*. Croatia: InTech.
34. Legrand, P. (2012). *Influence des conditions de fonctionnement de la pile à combustible.* Ph.D. Thesis l'École Doctorale de Chimie et Sciences du Vivant, Université de GRENOBLE, France.
35. Ramos-Alvarado, B.; Hernandez-Guerrero, A.; Elizalde-Blancas, F.; and Ellis, M. (2011). Constructal flow distribution as a bipolar plate for proton exchange membrane fuel cell. *International Journal of Hydrogen Energy*, 36, 12965 -12976.
36. Cano-Andrade, S.; Hernandez-Guerrero, A.; von Spakovsky, M.R.; Damian-Ascencio, C.E.; Rubio-Arana, J.C. (2009). Current density and polarization curves for radial flow field patterns applied to PEMFCs (Proton Exchange Membrane Fuel Cells). *Energy*, 35, 920-927.
37. Falcao, D.S.; Gomes, P.J.; Oliveira, V.B.; Pinho, C.; and Pinto, A.M.F.R. (2011).1D and 3D Numerical Simulations in PEM fuel cell. *International Journal of Hydrogen Energy*, 36, 12486-12498.
38. Patankar, S.V. (1980). *Numerical heat transfer and fluid flow.* New York: Hemisphere.
39. Lum, K.W.; McGuirk, J.J. (2005). Three-dimensional model of a complete polymer electrolyte membrane fuel cell - model formulation, validation and parametric studies. *Journal of Power Sources*, 143,103-124.
40. Liu, H.; Li, P.; and Wang, K. (2013). Optimization of PEM fuel cell flow channel dimensions, mathematic modelling analysis and experimental Verification. *International Journal of Hydrogen Energy*, 38, 9835-9846.
41. Chiang, M.S; and Chu, H.S. (2006).Numerical investigation of transport component design effect on a proton exchange membrane fuel cell. *Journal of Power Sources*, 160,340-352.
42. Khazaee, I.; Ghazikhani, M. (2012). Numerical simulation and experimental comparison of channel geometry on performance of a PEM fuel cell. *Arabian Journal for Science and Engineering*, 37, 2297-2309.